General Disclaimer

One or more of the Following Statements may affect this Document

- This document has been reproduced from the best copy furnished by the organizational source. It is being released in the interest of making available as much information as possible.

- This document may contain data, which exceeds the sheet parameters. It was furnished in this condition by the organizational source and is the best copy available.

- This document may contain tone-on-tone or color graphs, charts and/or pictures, which have been reproduced in black and white.

- This document is paginated as submitted by the original source.

- Portions of this document are not fully legible due to the historical nature of some of the material. However, it is the best reproduction available from the original submission.

Produced by the NASA Center for Aerospace Information (CASI)

the
ohio
state
university

research foundation
1314 kinnear road
columbus, ohio
43212

STUDIES OF HEAT SOURCE DRIVEN NATURAL CONVECTION

F.A. Kulacki and A.A. Emara
Department of Mechanical Engineering
The Ohio State University
Columbus, Ohio 432]0

STUDIES OF HEAT SOURCE DRIVEN NATURAL CONVECTION

by

F. A. Kulacki and A. A. Emara
Department of Mechanical Engineering
The Ohio State University
Columbus, Ohio   43210

FOREWORD

The work reported herein was sponsored by the National Aeronautics and Space Administration, Theoretical Studies Branch, Ames Research Center, Moffett Field, California, under Grant NGR-36-008-205. The experimental work was performed by A. A. Emara in partial fulfillment of the requirements for the degree of Doctor of Philosophy at The Ohio State University. Experiments are continuing with the objective of measuring temperatures within an internally heated horizontal fluid layer in developing convection. Analytical work is also underway and is aimed at a prediction of steady-state Nusselt numbers in the low-Rayleigh-number regime of convection.

ABSTRACT

Natural convection energy transport in a horizontal layer of internally heated fluid has been measured for Rayleigh numbers from 1.89×10^3 to 2.17×10^{12}. The fluid layer is bounded below by a rigid zero-heat-flux surface and above by a rigid constant-temperature surface. Joule heating by an alternating current passing horizontally through the layer provides the uniform volumetric energy source. The overall steady-state heat transfer coefficient at the upper surface is determined by measuring the temperature difference across the layer and power input to the fluid.

The correlation between the Nusselt and Rayleigh numbers for the data of the present study and the data of the Kulacki et al.[3] study is

$$Nu_1 = 0.389 \ Ra^{0.228} \ ,$$

where

$$1.89 \times 10^3 \leq Ra \leq 2.17 \times 10^{12}$$

$$2.75 \leq Pr \leq 6.85$$

$$0.025 \leq L/X \leq 0.50 \ .$$

By extrapolation to the conduction limit of $Nu_1 = 2$, this correlation predicts a critical Rayleigh number of 1314, which is within -2.2% of the value predicted by linear stability theory when the thermal coupling between the layer and its boundaries are taken into account.

TABLE OF CONTENTS

LIST OF FIGURES

LIST OF TABLES

NOMENCLATURE

A	Area of heat transfer surface
C	Constant of correlation for overall heat transfer
c_p	Specific heat at constant pressure of fluid
f	Fractional experimental uncertainty
g	Constant of gravitational acceleration corrected to latitude of The Ohio State University, 980.171 cm/s^2
h	Heat transfer coefficient, $q_{wall}/\Delta T$
H	Volumetric rate of energy generation in fluid
k	Thermal conductivity of fluid
L	Height of fluid layer
m,n	Constants of correlation for overall heat transfer
Nu	Nusselt number, hL/k
Nu_c	conduction value of Nusselt number
Nu^*	Nu/Nu_c
P	Power input to fluid
P_{loss}	Power loss due to heat leaks through side walls
Pr	Prandtl number, ν/α
q_{wall}	Heat flux at the wall
Ra	Rayleigh number $(g\beta/\alpha\nu)\ L^3\ (HL^2/2k)$
T	Temperature
ΔT	Maximum temperature difference, $T_0 - T_1$
w	Weight fraction of silver nitrate per weight of water
X	Characteristic horizontal dimension (smallest horizontal dimension of test cell
z	Vertical coordinate, $0 \leq z \leq L$

Greek Symbols

α Thermal diffusivity

β Isobaric coefficient of thermal expansion

μ Dynamic viscosity

ν Kinematic viscosity

ρ Density

Subscripts

c Critical value or conduction value

0 Evaluated at lower wall

1 Evaluated at upper wall

wall   Evaluated at wall

max   Maximum value

INTRODUCTION

Natural convection occurs frequently in fluid systems warmed internally by a distributed volumetric energy source. Such an energy source may be the absorption of incident radiation in a dense planetary atmosphere or the release of energy in a confined fluid by an exothermic chemical or nuclear reaction. Natural convection produced by distributed volumetric energy sources is consequently of importance in a wide range of scientific and engineering disciplines; e.g., geophysics, planetary physics, meteorology, astrophysics, environmental engineering, nuclear power technology, food processing, and chemical technology.

With regard to convection in planetary interiors, it should be noted that laboratory study of steady and unsteady natural convection with distributed energy sources provides particularly useful information for developing planetary thermal history models. The moon provides an interesting case study in this respect since pertinent geophysical data are relatively abundant, and the constraints imposed by its topography create a much less complex situation for analysis than those for the earth. However, an incomplete knowledge of the convective processes within the moon makes accurate thermal history analysis difficult.

In fluid layers with internally distributed energy sources, the conduction regime is characterized by a nonlinear temperature distribution. The maximum temperature difference within the fluid is directly and simply related to the strength of the energy source. When the energy source strength is increased above a certain critical value (i.e., above a "critical" value of Rayleigh number), destabilizing buoyant forces overcome stabilizing viscous forces and convective motion begins in that region of the fluid in which a negative mean temperature gradient exists. As the strength of the energy source is increased still further, the flow proceeds through a laminar (cellular) regime to the chaotic turbulent regime in which nearly all of the fluid layer is affected by the convective energy transport process.

Several problems for study can be identified in view of the above sequence of physical processes as the Rayeligh number is increased. These are (1) prediction of the critical Rayleigh number at which convection begins, (2) determination of steady temperature and velocity fields for both the laminar and turbulent regimes of flow, (3) determination of heat transfer rates with the fluid for both the laminar and turbulent regimes of flow, and (4) determination of developing temperature and velocity profiles for unsteady or developing convection. Past analytical and experimental work has addressed these problems, but understanding of heat-source-driven convection is not complete and not nearly at the same level as that of Benard convection, which has received considerably more attention in the past 25 years. A review of analytical and experimental work on heat source driven convection is given by Peckover[1] and Peckover and Hutchinson.[2] Additional reviews of recent work on heat source driven convection are given by Kulacki, Nagle and Cassen[3] and Kulacki and Emara.[4]

The experimental work reported here is part of a continuing study of heat-source-driven natural convection which is aimed at obtaining fundamental information on the thermal processes occurring in horizontal fluid layers with uniformly distributed energy sources. Overall heat transfer coefficients for steady convection in the turbulent and laminar regimes of flow have been obtained for a layer of low aspect ratio with a rigid insulated lower boundary and a rigid constant temperature upper boundary. Limited data on temperature within the layer for developing convection at low Rayleigh number have also been obtained. It is believed that the results of this kind will permit verification of limiting case models of unsteady convective processes occurring in planetary interiors and in certain other technological heat transfer problems.

EXPERIMENTAL APPARATUS AND PROCEDURE

EXPERIMENTAL APPARATUS

The experimental apparatus comprised a horizontal fluid layer bounded on the bottom by a rigid zero-heat-flux surface and on the top by a constant-temperature plate. For measurements at high Rayleigh numbers, a test cell of horizontal dimensions 50.8 x 50.8 cm was used. For very low Rayleigh number measurements, a test cell of horizontal dimensions 25.4 x 25.4 cm was used. In either cell, the layer depth was varied using spacers of different lengths.

Two of the side walls of each cell were 1.27 cm thick Plexiglas, and the other two side walls were formed by silver-plated electrodes for the passage of 60 Hz alternating current through an aqueous $AgNO_3$ solution. The bottom plate was 1.9 cm thick Plexiglas. A nickel-chromium resistance heater was imbedded in this bottom plate to help maintain a zero heat flux boundary condition. The top, bottom, and side walls of the cell were further insulated by a 5.08 cm thick layer of Fiberglas (see Fig. 1 for additional details).

The top plate for each cell was machined from an aluminum plate 2.54 cm thick. The plate was cut square to the dimensions of the cell minus 0.0762 cm on each side to allow room for the plate to slide into the cell. Channels were machined into this plate in a double-pass spiral pattern to allow cooling water to be circulated through the plate. The channels were 1.91 cm deep in the large cell and 2.22 cm deep in the small cell. A 0.635 cm plate was fixed to the backside of each channeled plate to provide a seal for the cooling water. Silicone rubber cement was used as a gasket material. The surface of each plate was faced on a lathe to a flatness of less than ±0.0025 cm and covered with a 0.0051 cm thick sheet of pressure-sensitive Mylar. The Mylar sheet provided electrical insulation between the top plate and the fluid layer.

When the plate was placed into the test cell, it rested on four spacers, each machined to ±0.00127 cm of a specified length. For moderate Rayleigh number, the spacers were of 2.54 cm diameter Plexiglas while for Rayleigh numbers greater than 10^{11}, the spacers were of 1.19 cm diameter glass.

Thermocouple wells, each 0.32 cm in diameter, were drilled into the top and bottom plates to within 0.128 cm from the surfaces in contact with the fluid. The wells were spaced uniformly on the plate to obtain spatially averaged measurement. All thermocouples were painted with General Electric No. 1202 insulating varnish. Thermocouples in the bottom plate were secured in their wells with epoxy cement; thermocouples in the top plate were secured in their wells with Teledyne, Technical "G" Copper Oxide Cement. The insulating varnish and copper oxide cement produced a resistance of 10^7 Ω between the thermocouples and the aluminum top plate.
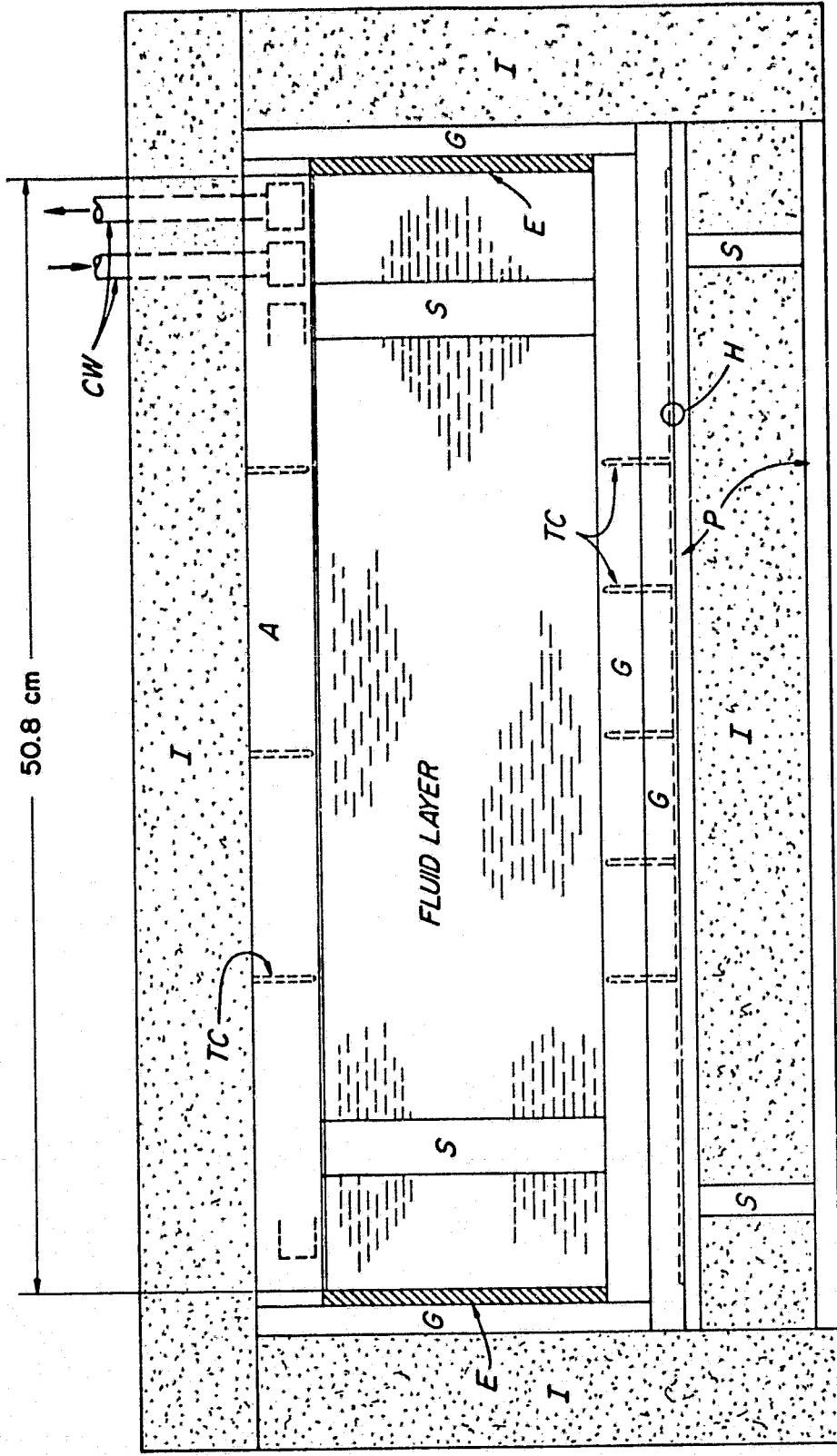
Figure 1. Detail view of convection cell

LEGEND

A   Aluminum   P   Plywood
CW Cooling Water   G   Plexiglas
E   Electrodes   H   Resistance Heater
I   Insulation   TC Thermocouple Well
                      S   Spacer

50.8 cm

FLUID LAYER

To measure the temperature difference across the layer, six copper-constantan thermocouples each in the top and bottom plates were connected in parallel. The output of each parallel circuit was determined relative to a reference thermocouple at 0°C. The difference in the two millivolt outputs determined in this way gave a reliable measurement of the temperature difference across the fluid layer.

The thermocouple arrangement for determining the heat flux through the bottom plate was a differencing thermopile using 20 thermocouples. Ten thermocouples were spaced across the bottom plates at 0.128 cm from the fluid surface and the other ten thermocouples were spaced across the bottom plate at 1.398 cm from the fluid surface. Thus, the output of the thermopile was interpreted as temperature difference across the material. This thermopile arrangement served as an indicator to determine when heat was being conducted into or out of the fluid layer through the lower surface.

A Leeds and Northrup Type K-3 universal potentiometer, in conjunction with a Leeds and Northrup 9834 Electronic dc null detector, was used to measure all thermocouple outputs. The total error of this arrangement is ±0.015% of reading +0.5 μV. For measurements made in this study, this would amount to ±0.014°C.

For Rayleigh numbers less than 3×10^9, a Sorenson Model 3000-S ac voltage regulator connected to a 110 V laboratory supply line was used to supply the power consumed in the fluid layer. The output of the voltage regulator was passed through a Variac so that regulation of power input to the test cell could be maintained.

An electrical schematic of the fluid layer would appear as a capacitor-resistor-capacitor in series. Therefore, in calculating the power input to the electrodes, the impedance angle might be significantly greater than zero. For this reason, it was decided to use a wattmeter transducer for measuring power input. The transducer chosen was an F. W. Bell Model HX-2014W which uses a Hall element to take into account the impedance angle. The transducer was calibrated by the manufacturer. A Fluke Model 8120-A digital multimeter was used to measure the output from the wattmeter transducer. This meter had a 4.5 digit display capacity and a published error of ±0.05% of input +20 μV. For a 50 W input to the fluid layer, this would amount to ±0.028 W. The instrument was certified by the manufacturer to be within published specifications.

For Rayleigh numbers greater than 3×10^9, large power inputs to the fluid layer were required which exceeded the capacity of the wattmeter transducer and the 110 V supply line. Therefore a 220 V supply line in conjunction with two transformers was used to provide regulated power. The 220 V line was connected to a step-down transformer (220/110 V). The output of this transformer was connected to the Sorenson regulator; the output of the regulator was then connected to a step-up transformer (110/220 V). The output of this transformer was connected

5

to a Variac to regulate the voltage applied to the fluid layer. A calibrated wattmeter was used to measure the power consumed in the test cell. Its reading was continually checked with independent voltmeter and ammeter readings for each run. The voltmeter and ammeter readings agreed with the wattmeter readings.

A constant-temperature bath was used to supply cooling water to the constant-temperature top plate in the test cell. Supply water temperature to the top plate did not vary from the desired setting by more than 0.1°C. In the high Rayleigh number experiments of this study, it was necessary to provide additional external cooling water to the constant temperature bath. This cooling water was supplied from the building supply and circulated through cooling coils contained in the bath.

Figure 2 is a schematic diagram of the experimental apparatus and instrumentation. Additional details on the test set-up are given by Kulacki, Nagle, and Cassen.[3]

EXPERIMENTAL PROCEDURE

Prior to each run, all reference thermocouples were placed in a 0°C ice bath and the interior portions of the test cell were cleaned with demineralized water. The electrode surfaces were polished with silver polish and were then wiped clean with acetone to remove any residue.

The initial horizontal alignment of the convection cell was accomplished by adjusting the legs on the triangular stand on which the cell rested. Fine horizontal alignment was accomplished with the Fell precision level placed on top of the bottom plate. The sensitivity of this level was 0.00416 cm/m.

The four spacers were spaced around the cell at the corners to support the top plate. The convection cell was then filled at a very slow rate with demineralized water to a level even with the top of the spacers. A conductivity meter attached to the top of the demineralizer indicated the specific resistance of the demineralized water was greater than 10^6 Ω. The desired quantity of reagent grade silver nitrate crystals was measured out with an analytical balance to ± 0.001 g and then dissolved in the demineralized water. Because of the large quantity of water in the fluid layer, the convection cell was used as a mixing chamber for forming the silver nitrate solution. Since Rayleigh numbers in this study were greatly in excess of the critical value and most of the mean heat transfer measurements were in the turbulent regime, any nonuniformities in the concentration of silver nitrate would be minimized by convective mixing within the layer. In addition, the long flow development time needed for mean heat transfer measurements with large plate spacings would act in favor of reducing nonuniformities in silver nitrate concentration.

6

Figure 2. Schematic diagram of experimental apparatus

The top plate was brushed with melted paraffin at its corners and at any other apparent breaks in the Mylar film to ensue that no fluid would come in contact with the aluminum top plate. The top plate was then eased very carefully into the convection cell. When the plate came into contact with the top surface of the fluid it was tilted slightly at an angle and then allowed to settle down flat on top of the spacers. It was necessary to tilt the plate in this manner to allow trapped air bubbles to escape.

The insulation was then placed on the side walls of the test cell, and the fluid layer was allowed to reach thermal equilibrium with the top plate. The power was then applied to the cell and adjusted to the required level for the Rayleigh number desired. A period of time much greater than that required by heat conduction theory to establish a conduction temperature profile was then allowed to elapse before recording data. Typically a period of five to eight hours was required to establish steady state for the highest Rayleigh number runs of this study. At least four readings of temperature of both upper and lower boundaries were taken and averaged. Another set of four readings was taken and averaged one-half hour later in order to ensure that steady state had been obtained. When good agreement was reached, the data were recorded.

The high Rayleigh number runs of this study required constant monitoring of boundary temperatures since with the high power dissipation in the fluid (up to 2.5 kW in some cases), the mean temperature of the test cell and insulation did not reach a constant value until near the end of the flow development time allowed. Thus, the high Rayleigh number runs were characterized by a continuous drift in mean temperature of the system; the top plate temperature and the guard heater in the bottom plate had to be adjusted during the flow development period so that the desired thermal boundary conditions could be maintained. Near the end of the flow development period, small adjustments in the top plate temperature were found to produce no noticeable effects on the total temperature difference across the fluid layer.

RESULTS

The Nusselt number at the upper surface of the fluid layer was defined using the thickness of the layer, L, as the characteristic length scale and the temperature difference between the lower and uppe surfaces as the characteristic temperature difference. In terms of the power dissipated within the layer,

$$Nu_1 = \frac{(P - P_{loss})L}{kA(T_0 - T_1)} \qquad (1)$$

Heat transfer results were first correlated in the form

$$Nu_1 = C\ Ra^m . \qquad (2)$$

The thermophysical properties of the fluid were in all cases evaluated at the top plate temperature. Appendix A presents a summary of the thermophysical property values for dilute aqueous silver nitrate solutions. The experimental data are presented in Appendix B.

A linear regression of $\ell n(Nu_1)$ on $\ell n(Ra)$ gave the following correlations over the indicated range of Rayleigh numbers for the data of this study:

$$\left. \begin{array}{c} Nu_1 = 0.403\ Ra^{0.226} \\[4pt] 1.05 \times 10^4 \leq Ra \leq 2.17 \times 10^{12} \\[4pt] 2.75 \leq Pr \leq 6.85 \\[4pt] 0.025 \leq L/X \leq 0.50 \end{array} \right\} \qquad (3)$$

$$\left. \begin{array}{c} Nu_1 = 0.383\ Ra^{0.230} \\[4pt] 1.89 \times 10^3 \leq Ra \leq 10^5 \\[4pt] 6.18 \leq Pr \leq 6.75 \\[4pt] 0.025 \leq L/X \leq 0.0375 \end{array} \right\} \qquad (4)$$

$$\left. \begin{array}{c} Nu_1 = 0.396\ Ra^{0.227} \\[4pt] 1.89 \times 10^3 \leq Ra \leq 2.17 \times 10^{12} \\[4pt] 2.75 \leq Pr \leq 6.85 \\[4pt] 0.025 \leq L/X \leq 0.50 \end{array} \right\} \qquad (5)$$

Additional correlations of the data are presented in Appendix C. The experimental data and the correlations for the laminar and turbulent regimes of flow, Eq. (3), are presented graphically in Fig. 3. It may be noted from Fig. 3 that the scatter in the data increases significantly for $Ra < 10^4$. This is due to external effects (e.g., room temperature changes) which could not be completely damped out by the small test cell and its insulation. Convection at $Ra \leq 10\,Ra_c$ is quite feeble, and any externally imposed disturbance can be expected to influence the flow and energy transport rate. Kulacki and Goldstein[5] also observed an increase in scatter at low Rayleigh number in their study of a layer with two constant temperature boundaries. It appears that in the present study the trend in the Nusselt-versus-Rayleigh number curve is well established for $Ra \geq 10^4$ since the data for $10^3 < Ra \leq 10^4$ have but little effect on the constants of correlation [compare Eq. (3) with Eq. (5)].

Assuming that a correlation of the form of Eq. (2) holds in the vicinity of the critical Rayleigh number, it can be used to estimate Ra_c by extrapolation to the conduction value of $Nu_1 = 2$. Equation (3) in this way gives a critical Rayleigh number of 1161; Eq. (5) predicts a critical Rayleigh number of 1254. Equation (4) is not used as a predictor of Ra_c because of the large amount of scatter in the data for $Ra < 10^4$ (see Fig. 12).

To compare existing theoretical predictions of Ra_c to the above measured values, it is necessary to take into account the thermal coupling between the fluid layer and its environment. This coupling is expressed theoretically by the Biot number, $Bi = h_{external}L/k_f$. For the test cells constructed for this study, an equivalent Biot number, Bi^+, is defined as the ratio of the thermal conductance of the bounding wall to that of the fluid layer; $Bi^+ = (k_w/L_w)/(k_f/L)$, where the conductance of the wall is obtained from the additive thermal resistance concept for a composite slab. For both the large and small cells, $L = 1.27$ cm at the lowest Ra measured. Using nominal literature values for the material properties of the layer boundaries, $Bi^+ \approx 64.0$ for the large cell and $Bi^+ \approx 67.1$ for the small cell. At a Biot number of 65, the linear theory stability limit is $Ra_c = 1344$.[6] Thus, the values of critical Rayleigh number given by Eq. (3) is within -13.5% of the theoretically determined value while that of Eq. (5) is within -6.7%. This agreement between the measured and theoretical critical Rayleigh numbers is particularly good since the thermal boundary conditions of the experimental apparatus do not exactly match the idealized thermal boundary conditions of the theory.

By combining the data of the present study with the data of Kulacki et al.,[3] a linear regression of $\ell n(Nu_1)$ on $\ell n(Ra)$ gives
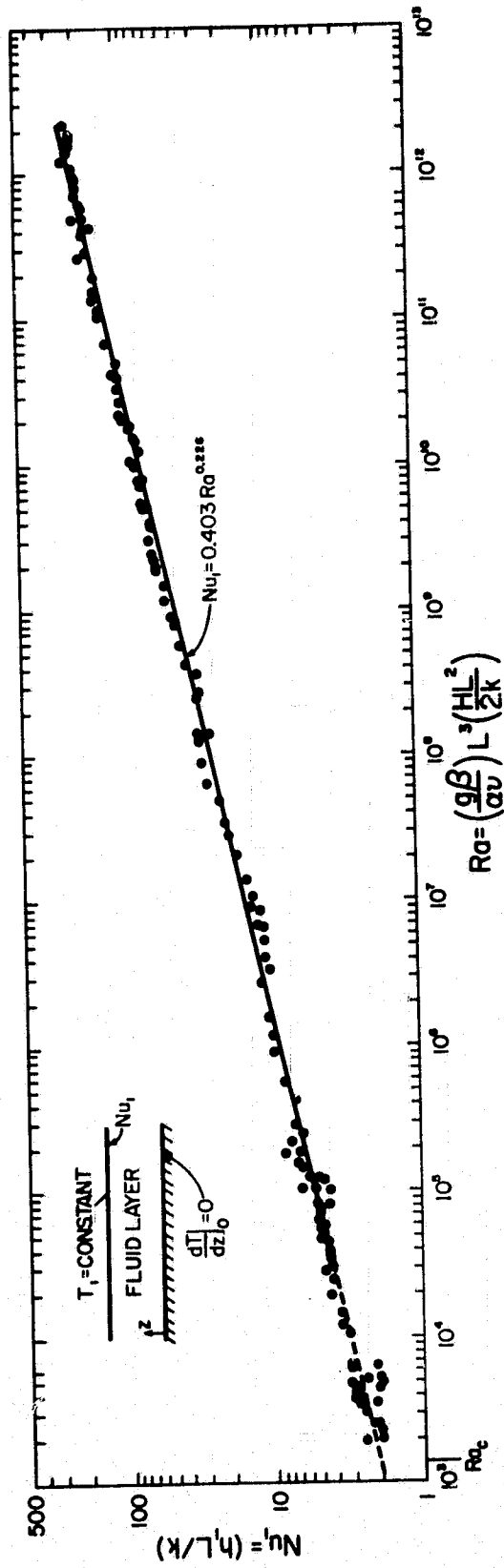
Figure 3. Experimental heat transfer data

11

$$\overline{Nu}_1 = 0.389 \ Ra^{0.228}$$

$$1.89 \times 10^3 \le Ra \le 2.17 \times 10^{12}$$

$$2.75 \le Pr \le 6.85$$

$$0.025 \le L/X \le 0.50$$

(6)

Equation (6) gives a measured value of the critical Rayleigh number of 1314. This estimate is within -2.2% of the theoretical value of linear stability theory.

The steady-state heat transfer data were analyzed for the existence of the so-called "discrete transitions" in heat flux. Such transitions are known to exist for convecting layers which are heated from below and from within. Rayleigh numbers at which transitions in heat flux occur are found by plotting the heat transfer data in the form $Ra \cdot Nu_1$ versus Ra over a limited range of Ra on Cartesian coordinates. It is the nature of such a plot to smooth the data in a way that accentuates changes in the slopes of straight lines fit to the data. The Rayleigh numbers at which discrete changes in slope occur are termed the "transition" Rayleigh numbers. Kulacki et al.[3] reported the existence of five transitions in heat flux for $4.2 \times 10^5 < Ra \le 1.4 \times 10^9$. The transition Rayleigh numbers of the present study are listed in Table 1 along with those of Kulacki and Nagle. Figures 4-11 graphically depict these transition Ra.

Table 1. Transition Rayleigh Numbers

This Study	Kulacki et al.[3]
4.2×10^5	4.2×10^5
6.1×10^6	4.9×10^6
2.0×10^7	3.0×10^7
3.3×10^8	4.0×10^8
1.5×10^9	1.4×10^9
1.5×10^{10}	
6.5×10^{10}	
3.6×10^{11}	

The agreement between the transition Rayleigh numbers of the present and Kulacki, Nagle and Cassen studies is quite good; and the results of the present study essentially confirm the transition Rayleigh numbers of Kulacki et al.
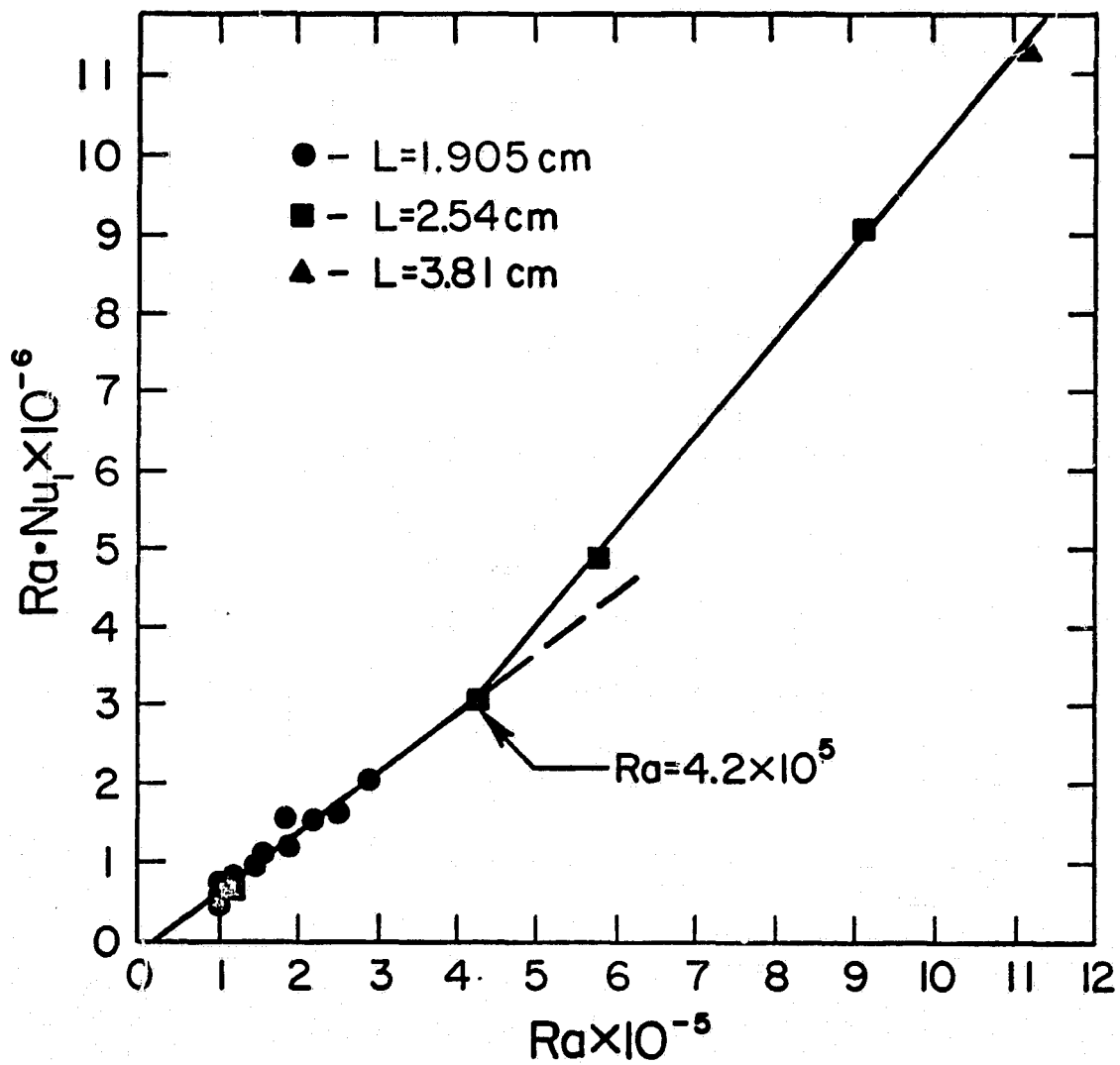
Figure 4.   Transition Rayleigh number at Ra = 4.2 x 10⁵
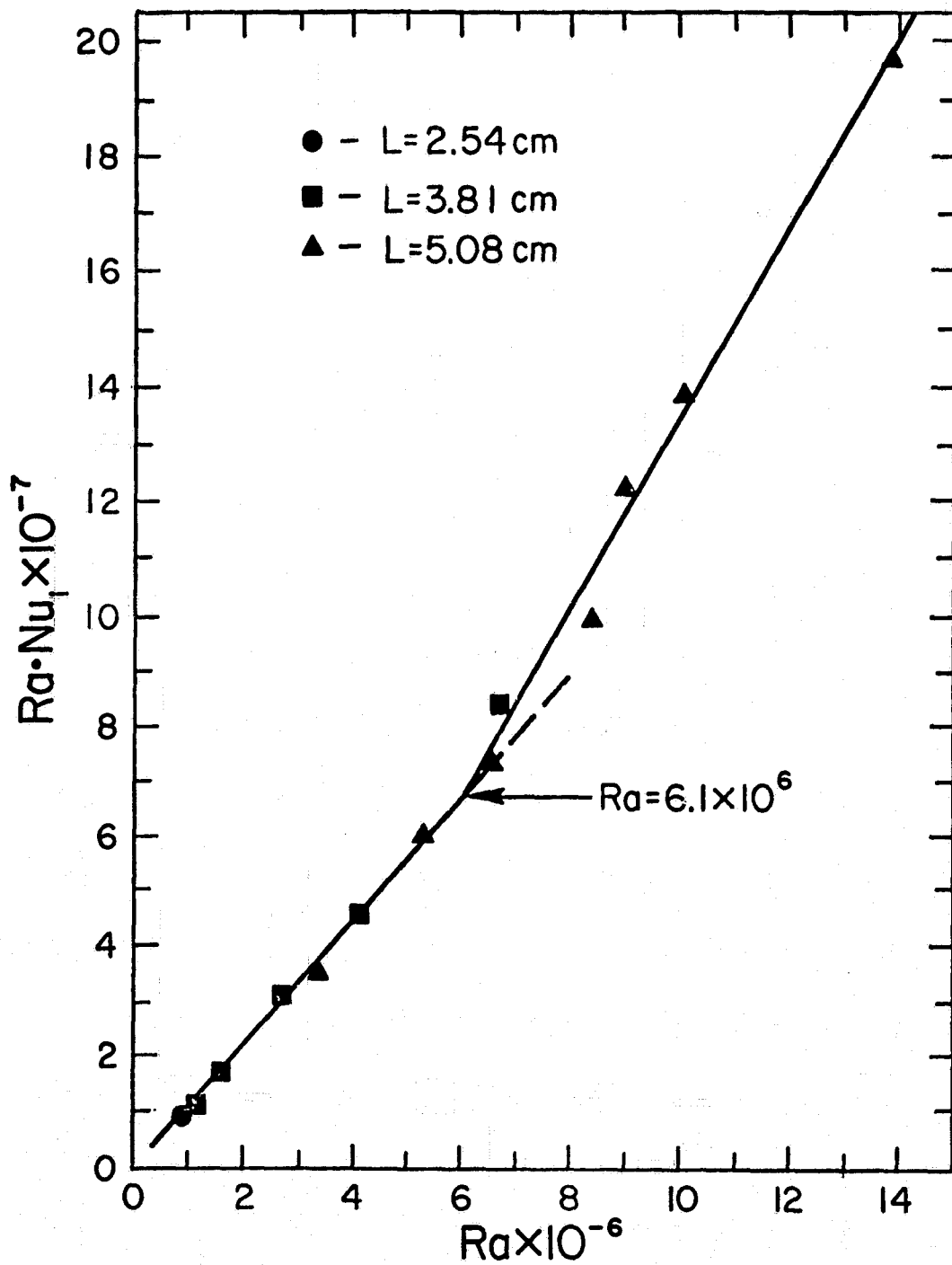
Figure 5. Transition Rayleigh number at Ra = 6.1×10^6

14
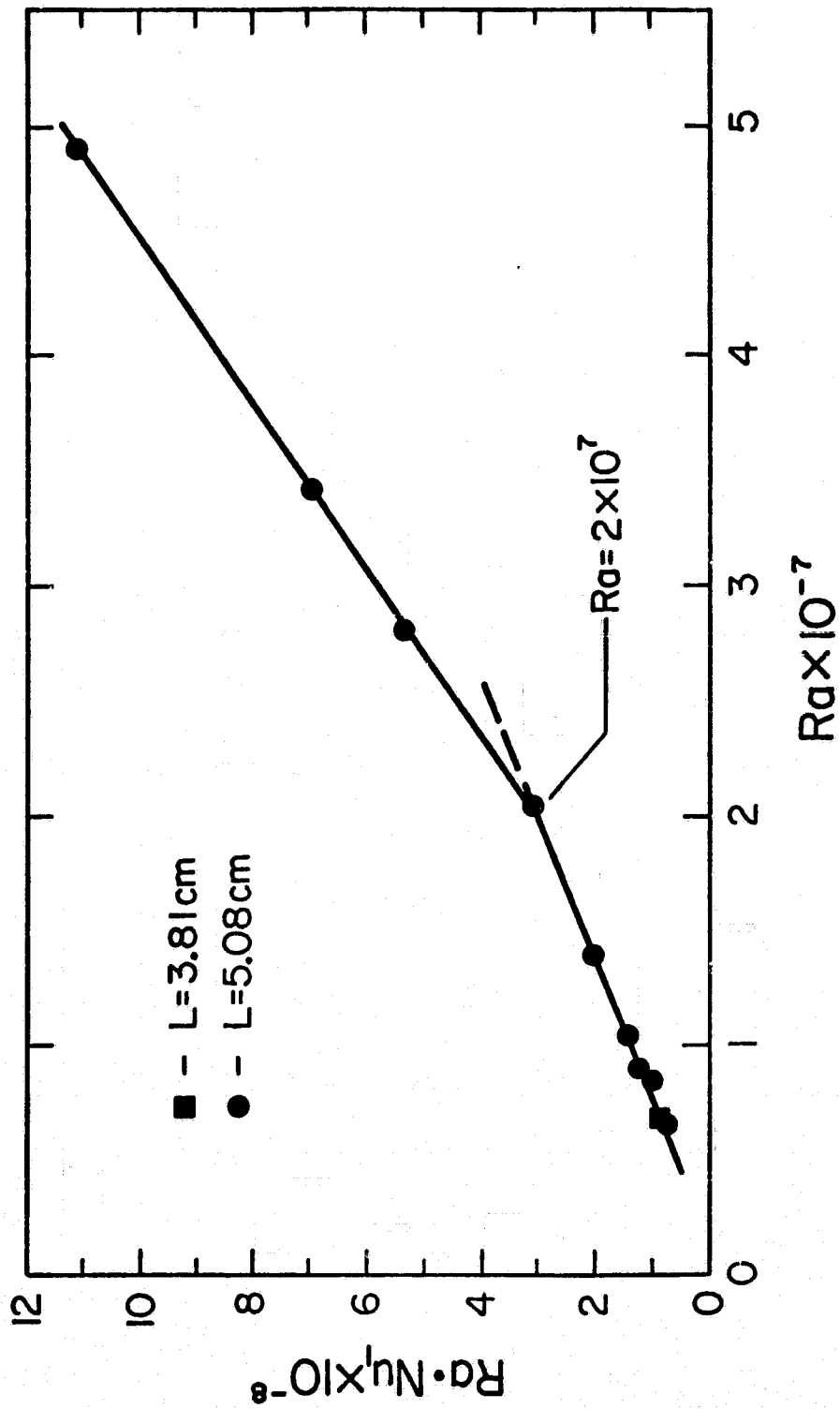
Figure 6. Transition Rayleigh number at Ra = 2.0 x 10^7
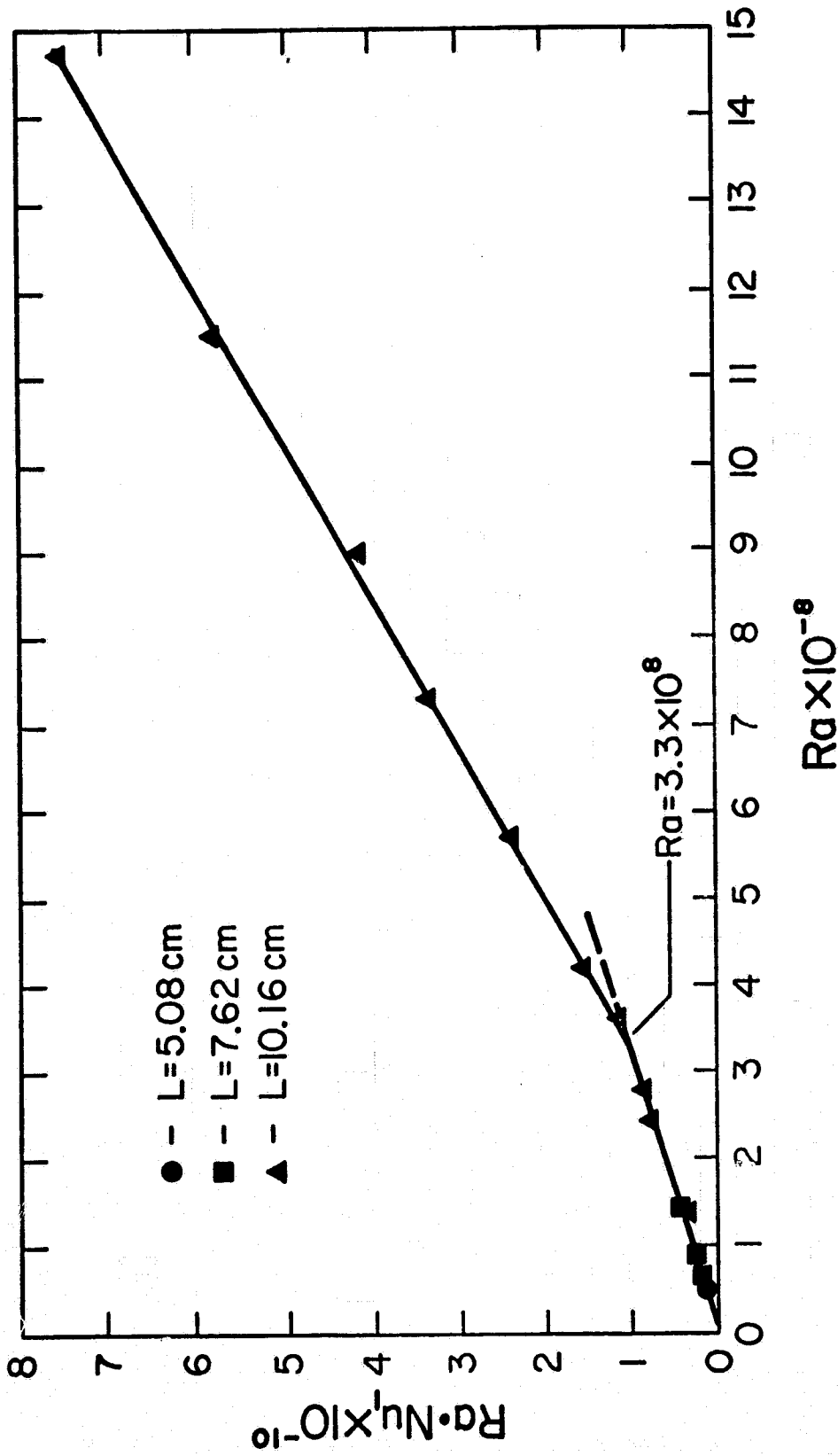
Figure 7. Transition Rayleigh number at Ra = 3.3×10^8
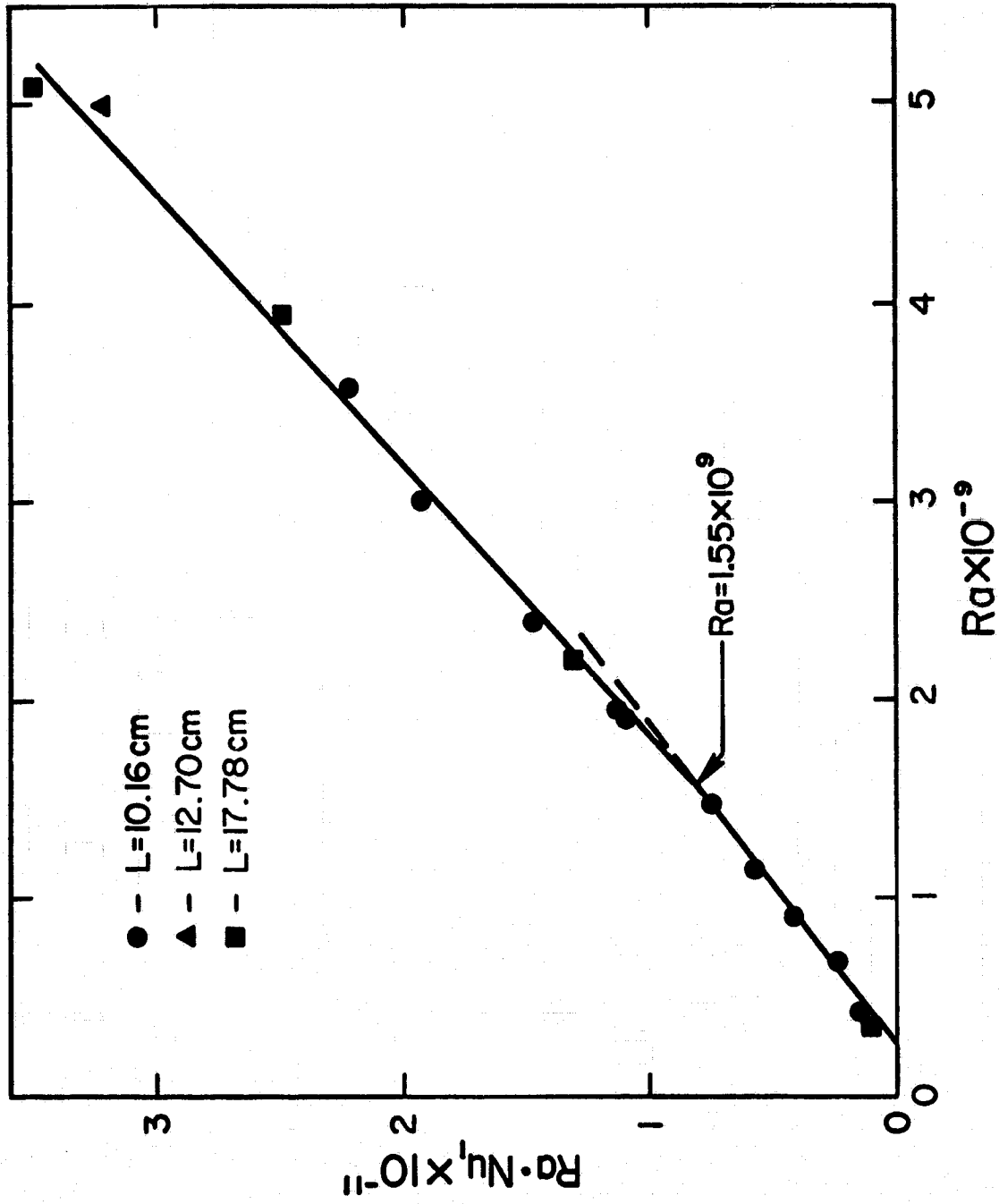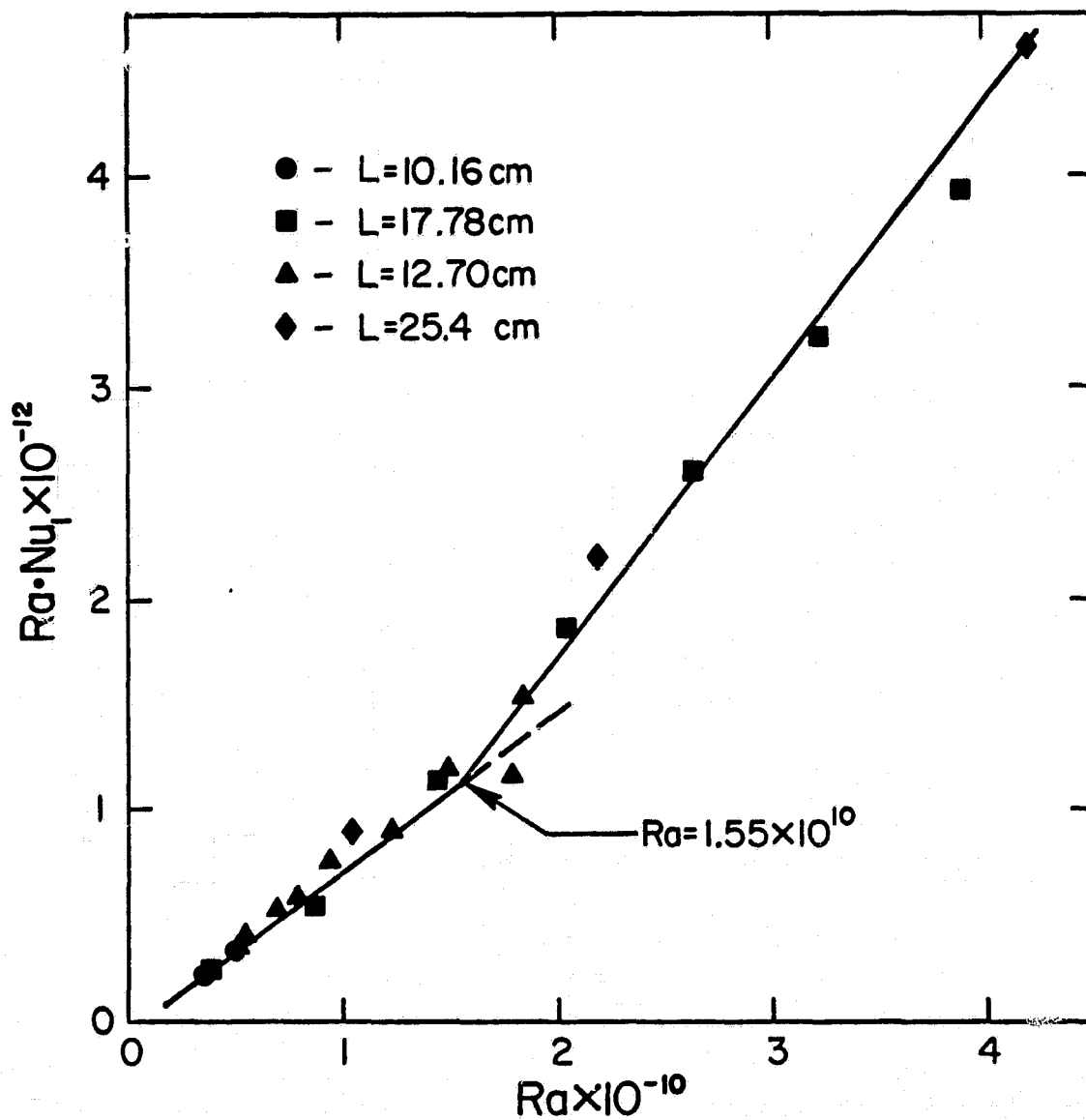
Figure 8. Transition Rayleigh number at Ra = 1.55 x 10⁹

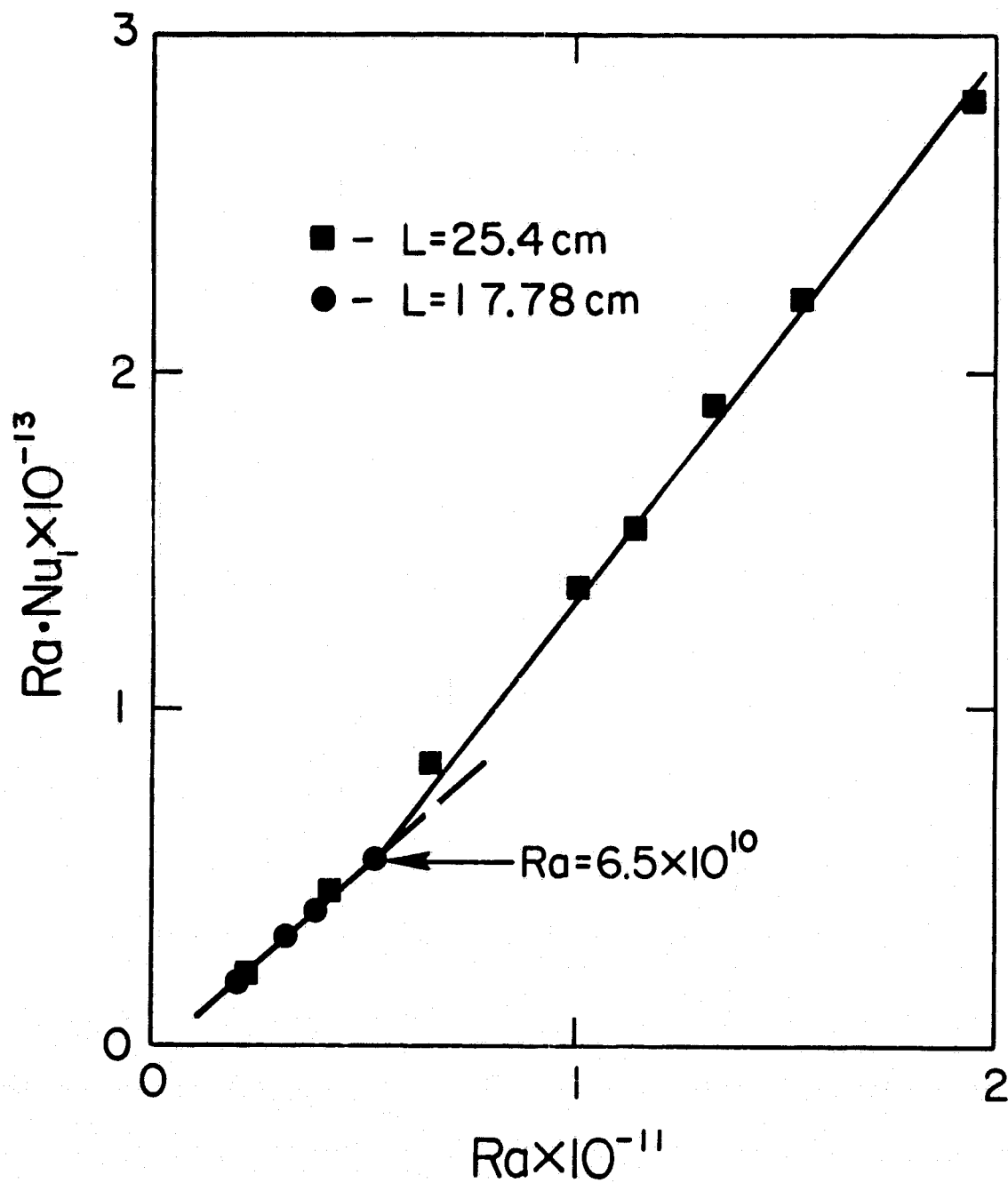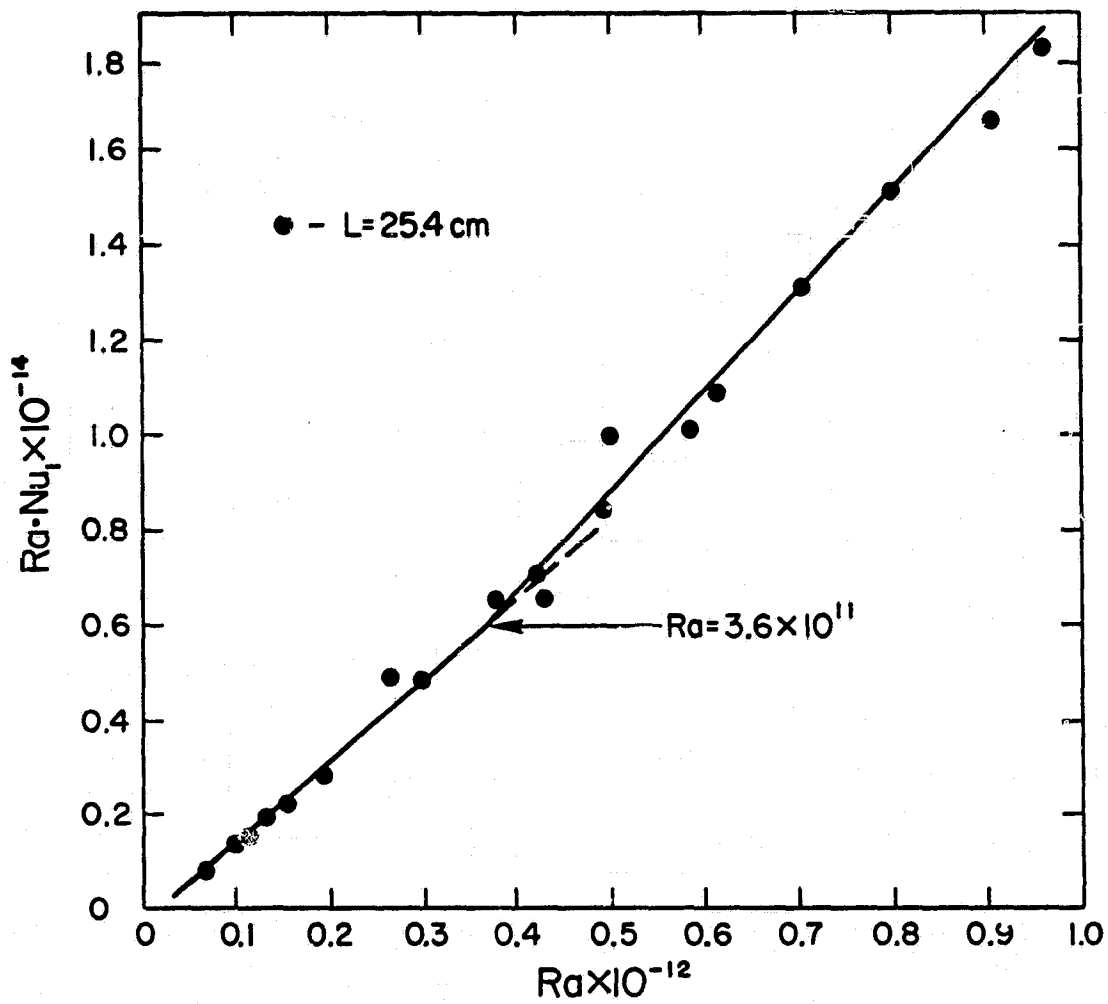Figure 9. Transition Rayleigh number at Ra = 1.55 x 10^{10}

Figure 10. Transition Rayleigh number at Ra = 6.5 x 10¹⁰

Figure 11. Transition Rayleigh number at Ra = 3.6 x 10^{11}

DISCUSSION

The present study essentially extends the heat transfer results of Kulacki et al.[3] to near the conduction regime and to Rayleigh numbers which are 10^9 times the critical values of linear stability theory. At these Rayleigh numbers, turbulent convection can be considered fully developed. The high Rayleigh number data of the present study appear to be the first obtained in controlled laboratory experiments.

The correlation for heat transfer, including the data of the present study and that of Kulacki et al.,[3] is

$$
\left.
\begin{aligned}
Nu_1 &= 0.389 \ Ra^{0.228} \\
1.89 \times 10^3 &\leq Ra \leq 2.17 \times 10^{12} \\
2.75 &\leq Pr \leq 6.85 \\
0.025 &\leq L/X \leq 0.50
\end{aligned}
\right\} . \tag{7}
$$

This correlation, when extrapolated to the conduction limit of $Nu_1 = 2$, gives a critical Rayleigh number of 1314; this value is within -2.2% of the critical Rayleigh number predicted by linear stability theory[6] when the thermal coupling between the fluid layer and its boundaries is taken into account. This agreement between the theoretical and measured critical Rayleigh numbers is particularly good since the thermal boundary conditions in the experiments do not exactly match those of the theory. Furthermore, the agreement between the theoretical and experimental critical Rayleigh numbers of our study and of the Kulacki and Goldstein study[6] (i.e., the internally heated layer with two equal temperature boundaries) tend to confirm the linear stability theory as being sufficient for giving limits of instability in internally heated fluid layers.

The discrete transitions in heat flux found in this study essentially confirm those of Kulacki et al.[3] Three additional transition Rayleigh numbers (i.e., 1.5×10^{10}, 6.5×10^{10}, and 3.6×10^{11}) are also found in the present study. The transition at Ra = 3.6×10^{11} is, however, open to question as considerable scatter exists in the data (see Fig. 12). Additional experimental work is needed to confirm the existence of a transition in heat flux at this Rayleigh number.

The heat transfer results of the present study can be used, as were the results of Kulacki et al.[3] to estimate Nusselt numbers at the upper boundary of a layer with two equal temperature boundaries. Conceptually, the layer with two equal temperature surfaces is divided into two sub-layers separated by a plane of zero average heat flux. The heat transfer process in the upper sub-layer corresponds to that of the present study, with the exception that the lower hydrodynamic boundary condition is not that of a rigid surface. The lower sub-layer

can be assumed to be strongly dominated by conduction, but this is not essential to our development here. Baker, Faw, and Kulacki[7] have, however, used the assumption of lower sub-layer conduction to estimate both upward and downward heat transfer in layers with equal and unequal temperature boundaries. Their approach was to use results of the present study to compute the heat transfer in the upper sub-layer and to assume the downward heat transfer is by conduction only.

The thickness of the upper sub-layer, L^*, is given by the fraction of total heat generated that is transferred upward; thus

$$\frac{L^*}{L} = \frac{Nu_1}{Nu_1 + Nu_0} , \tag{8}$$

where Nu_1 and Nu_0 are taken from the Kulacki-Goldstein correlation.[5] Equation (8) can be written

$$\frac{L^*}{L} = \frac{0.3879 \, Ra^{0.236}}{0.3879 \, Ra^{0.236} + 1.524 \, Ra^{0.094}} . \tag{9}$$

When a value of the whole-layer Rayleigh number, Ra, is specified, Eq. (9) gives the length scale to be used in the Rayleigh number of Eq. (7). Thus the upper sub-layer heat transfer rate is given by

$$Nu_1 = 0.389 \, Ra^{0.226} \left(\frac{L^*}{L}\right)^{1.130} , \tag{10}$$

where Nu_1 is now based on L^*.

In Table 2, the Nusselt number at the upper surface, normalized by conduction values determined by the Kulacki-Goldstein correlation and Eq. (10), are compared.

Table 2 shows that the Nusselt numbers given by Eq. (10) are in fair agreement with those of the Kulacki-Goldstein correlation. The results of the present study [Eq. (7)] provide an ad hoc basis for the extension of the Kulacki-Goldstein correlation to higher Rayleigh numbers, especially when thermophysical data do not permit computation of exact values of Ra (e.g., in geophysical and nuclear technology applications). Backer, Faw, and Kulacki[7] have obtained similar results with essentially the same approach, although here we make no assumptions on the mechanism of energy transport in the lower sub-layer. The results of Table 2 are thus deductions based on whole-layer convection data applied to the layer with an insulated lower boundary.

The use of both the present correlation and the Kulacki-Goldstein correlation to develop simple models of the whole-layer problem call for further scrutiny and work, especially since the whole-layer convection correlations are valid for Rayleigh numbers up to just 675 times the critical values of linear stability theory. It would be desirable to obtain additional experimental data on the whole-layer problem for

Table 2. Upper Sub-layer Nusselt Number. $Nu_1^* = Nu_1/Nu_c$, where $Nu_c = 2$ for the Present Study and $Nu_c = 4$ for the Kulacki-Goldstein Correlation

Ra	Kulacki-Goldstein[5]			Present Study	
	Nu_1^*	Nu_0^*	L^*/L	$Ra \cdot (L^*/L)^5$	Nu_1^*
10^5	1.46	1.12	0.566	5.82×10^3	1.38
10^6	2.52	1.39	0.645	1.11×10^5	2.69
10^7	4.35	1.73	0.715	1.87×10^6	5.09
10^8	7.49	2.15	0.769	2.69×10^7	9.29
10^9	12.90	2.67	0.828	3.89×10^8	16.99
10^{10}	22.22	3.32	0.870	4.98×10^9	30.23
10^{11}	38.25	4.12	0.903	6.00×10^{10}	53.06
10^{12}	65.86	5.12	0.928	6.88×10^{11}	92.09

Rayleigh numbers of the order of 10^5 times the critical values to check the validity of Eq. (8).

The present study also presents new heat transfer data for what is generally regarded as the laminar regime of motion (see Tritton and Zarraga[8] and Schwab and Schwiderski[9]) and it is worthwhile to compare these results to the theoretical results of Roberts[10] and Thirlby.[11]

Thirlby[11] used a parameter defined as

$$M = \frac{\text{mean temperature difference across layer, no motion}}{\text{mean temperature difference across layer, motion}} \quad (11)$$

to characterize the energy transport within the layer. Roberts[10] used the reciprocal of this quantity. Our results can be directly related to M since, in terms of the physical parameters of the present study,

$$M = \frac{HL^2/2k}{\Delta T} . \quad (12)$$

Since $Nu_1 = HL^2/k\Delta T$

$$M = Nu_1^* . \quad (13)$$

Values of Nu_1^* (or M) versus Ra obtained by Roberts using the shape assumption and by Thirlby are plotted along with experimental data; the agreement between the experimental data and Roberts' results is fair over the entire Rayleigh number range of Figure 12, which includes that for feeble convection and fully developed

23
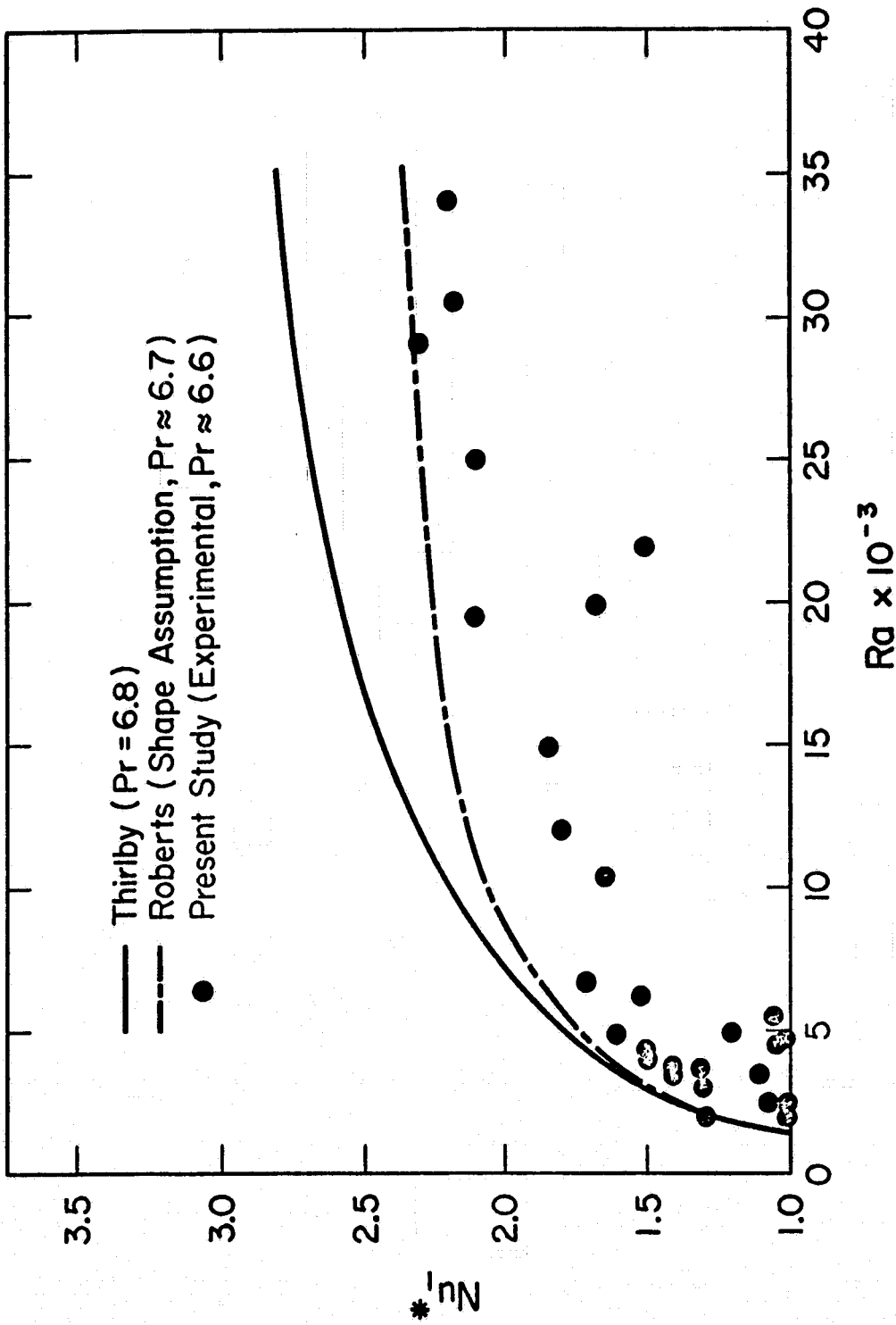
Figure 12. Nu_1^* as a function of Ra for laminar convection. Theoretical results (Thirlby[11] and Roberts[10]) are for roll solutions

laminar convection. The data and results of Roberts and Thirlby are in relatively good agreement for Ra $\lesssim$ 4000; in this range of Ra, the mean temperature profile is still very nearly parabolic, and any persistance of a preferred stable plan form of motion is quite likely. For this very limited range of Rayleigh numbers, the experiments seem to support the assumptions and hypotheses of both theoretical works. At higher Rayleigh numbers, agreement between experiment and theory is less perfect, even taking into account the scatter of the data. However, it is somewhat surprising that Roberts' result, which employed the shape assumption, lies closer to the experimental data than Thirlby's result, which is a steady-state limit of the unsteady convection problem using the method of artificial compressibility (see Chorin[13]). More precise experiments and a reexamination of the theory are needed to resolve these differences. It may be noted that each of the theoretical curves and the experimental data correspond to slightly different Prandtl numbers, but these differences are not considered significant here.

APPENDIX A

THERMOPHYSICAL PROPERTY VALUES

All of the thermophysical properties of the materials used in the design of the convection cell were taken either from suppliers' literature or from standard tabulated values.

The common thermophysical properties of the silver nitrate solution which served as the heat transfer medium in the convection cell were necessary for calculation of both the Rayleigh and Nusselt numbers. Since no attempts were made to precisely control the concentration of silver nitrate from run to run, it was necessary to evaluate these properties for concentration as well as temperature dependence. Computer subroutines used to calculate property values of the aqueous silver nitrate solution were adapted for use in this study from Kulacki.[4] These subroutines used least squares polynomial curve fits when sufficient single parameter data was available; otherwise, linear interpolation was used.

Least squares polynomial fits were developed for both concentration and temperature dependence for density and dynamic viscosity. Values of specific heat and thermal conductivity for pure water were used as functions of temperature alone since sufficient data for concentration dependence do not exist. Use of pure water values for specific heat and thermal conductivity results in errors of the order of 0.5% in these values.

The value of the thermal expansion coefficient was estimated from information available on the temperature and concentration dependence of solution density. Since the solution density is a smooth function of temperature and concentration, values of $-\frac{1}{\rho}\left[\frac{\partial \rho}{\partial T}\right]$ were estimated by linear interpolation between the value for pure water and the value at 1% dissolved silver nitrate. The value of the derivative $\left[\frac{\partial \rho}{\partial T}\right]$ was evaluated over a temperature interval of 0.10°C at the temperature of the upper surface. Using the value of the coefficient of thermal expansion of pure water would have resulted in at least a 1% error. The accuracy of the value used in this study was estimated to be of the order of 0.5-1%.

Table A-I gives a summary of temperature and concentration dependence of the thermophysical properties of aqueous silver nitrate solution. It may be noted that Table A-I presents the thermophysical property data in the temperature range 20-25°C. Since no reliable body of data is available at present for temperatures much in excess of 25°C, the computer programs which computed the data of Table A-I were used to obtain thermophysical property data at temperatures of interest in the present study for $Ra > 10^{10}$. This procedure is estimated to have introduced an additional 1% error in Rayleigh and Nusselt numbers for $Ra > 10^{10}$.

26

Table A-I - Thermophysical Properties of Aqueous Silver-Nitrate Solution

		Temperature (°C)					
Property	w	20	21	22	23	24	25
ρ	0.000	0.998527	0.998235	0.997943	0.997651	0.997359	0.997067
	0.005	0.998569	0.998277	0.997985	0.997693	0.997401	0.997109
	0.010	0.998611	0.998319	0.998027	0.997735	0.997443	0.997151
μ x 10²	0.000	1.008658	0.984578	0.961286	0.938764	0.916991	0.895948
	0.005	1.010556	0.986451	0.963135	0.940589	0.918794	0.900331
	0.010	1.012330	0.988208	0.964875	0.942312	0.920499	0.899418
β x 10³	0.000	0.206672	0.217220	0.227564	0.237704	0.247641	0.257375
	0.005	0.206846	0.217375	0.227701	0.237824	0.247745	0.257464
	0.010	0.207020	0.217530	0.227838	0.237944	0.247850	0.257554
c_p	0.000	4.179161	4.178592	4.178076	4.177612	4.177197	4.176831
k x 10²	0.000	0.597191	0.598869	0.600531	0.602178	0.603805	0.605423

Note that units are:

ρ - Density, g/cm^3
μ - Viscosity, g/s-cm
β - Coefficient of thermal expansion $1/°C$
c_p - Specific heat, W-s/g-°C
k - Conductivity, W/cm-°C

APPENDIX B

EXPERIMENTAL HEAT TRANSFER DATA

Table B-I - Experimental Heat Transfer Data

Run	Pr	L (cm)	P (W)	w	ΔT (°C)	$\dfrac{\Delta T}{(HL^2/2k)}$	Ra	Nu_1
161	6.59	1.270	0.336	0.0037	0.041	0.749	1.896×10^3	2.578
184	6.56	0.635	5.636	0.0041	0.469	1.011	2.009	1.980
185	6.56	0.635	6.245	0.0041	0.508	0.989	2.228	2.023
162	6.59	1.270	0.455	0.0037	0.068	0.914	2.565	2.131
186	6.56	0.635	7.091	0.0041	0.513	0.879	2.527	2.271
187	6.56	0.635	8.500	0.0041	0.535	0.765	3.031	2.613
188	6.56	0.635	9.818	0.0041	0.587	0.726	3.514	2.755
163	6.59	1.270	0.636	0.0037	0.097	0.932	3.588	2.100
189	6.55	0.635	10.26	0.0041	0.631	0.746	3.674	2.679
190	6.60	0.635	10.75	0.0041	0.619	0.698	3.775	2.863
191	6.60	0.635	11.45	0.0041	0.621	0.658	4.019	3.036
192	6.60	0.635	12.16	0.0041	0.661	0.659	4.271	3.036
164	6.59	1.270	0.791	0.0037	0.122	0.937	4.460	2.095
193	6.59	0.635	12.93	0.0041	0.687	0.645	4.545	3.099
194	6.69	0.635	13.66	0.0041	0.721	0.639	4.655	3.128
159	6.63	1.905	0.173	0.0050	0.013	0.858	4.867	1.960
195	6.69	0.635	14.55	0.0041	0.744	0.619	4.956	3.231
165	6.64	1.270	0.909	0.0037	0.122	0.815	5.035	2.422
160	6.63	1.905	0.191	0.0055	0.041	0.880	5.379	2.089
196	6.58	0.635	17.15	0.0041	0.844	0.597	6.065	3.348
166	6.59	1.270	1.127	0.0037	0.171	0.921	6.372	2.132
197	6.58	0.635	18.34	0.0041	0.895	0.592	6.495	3.376
170	6.57	1.270	1.856	0.0037	0.185	0.611	1.047×10^4	3.254
171	6.76	1.270	2.273	0.0037	0.210	0.559	1.207	3.567
172	6.75	1.270	2.718	0.0037	0.245	0.544	1.449	3.677
173	6.75	1.270	3.654	0.0037	0.281	0.466	1.948	4.299
115	6.28	1.270	12.73	0.0045	0.310	0.594	1.997	3.287
116	6.45	1.270	14.84	0.0045	0.402	0.658	2.20	3.010
174	6.61	1.270	4.473	0.0037	0.349	0.474	2.507	4.217
175	6.61	1.270	5.200	0.0037	0.367	0.428	2.915	4.677
148	6.71	1.270	5.618	0.0055	0.428	0.461	3.045	4.346
176	6.73	1.270	6.400	0.0037	0.482	0.456	3.433	4.392
149	6.71	1.270	6.964	0.0055	0.519	0.451	3.779	4.433
177	6.73	1.270	7.300	0.0037	0.548	0.454	3.916	4.405
063	6.28	1.905	5.550	0.0044	0.152	0.446	4.420	4.470
178	6.73	1.270	8.745	0.0037	0.582	0.403	4.699	4.969
150	6.71	1.270	9.236	0.0055	0.641	0.420	5.013	4.777
179	6.63	1.270	9.882	0.0037	0.658	0.403	5.494	4.955
064	6.30	1.905	7.410	0.0044	0.196	0.429	5.840	4.670
180	6.65	1.270	11.17	0.0037	0.004	0.709	6.179	5.205
028	6.50	2.540	2.750	0.0042	0.117	0.516	6.440	5.270
181	6.65	1.270	12.82	0.0037	0.832	0.393	7.089	5.092
065	6.30	1.905	9.890	0.0044	0.239	0.393	7.860	5.050
182	6.65	1.270	14.67	0.0037	0.893	0.369	8.117	5.426
090	6.25	1.905	10.29	0.0044	0.285	0.450	8.260	4.350

Run	Pr	L (cm)	P (W)	w	ΔT (°C)	$\frac{\Delta T}{(HL^2/2k)}$	Ra	Nu_1
093	6.25	1.905	12.58	0.0044	0.347	0.448	1.00×10^5	4.40
066	6.30	1.905	13.27	0.0044	0.245	0.300	1.06	6.650
155	6.69	1.905	3.855	0.0055	0.355	0.371	1.065	5.30
029	6.68	2.540	5.00	0.0042	0.207	0.502	1.210	4.690
094	6.26	1.905	15.45	0.0044	0.384	0.404	1.230	4.930
067	6.29	1.905	15.91	0.0044	0.348	0.355	1.260	5.810
068	6.36	1.905	19.98	0.0044	0.374	0.320	1.470	6.150
156	6.69	1.905	5.60	0.0055	0.391	0.282	1.546	7.066
070	6.27	1.905	22.90	0.0044	0.332	0.236	1.830	8.410
068	6.23	1.905	23.27	0.0044	0.438	0.306	1.880	6.350
071	6.85	1.905	26.85	0.0044	0.474	0.287	2.20	6.840
157	6.27	1.905	7.855	0.0055	0.599	0.310	2.508	6.414
158	6.60	1.905	10.13	0.0055	0.697	0.278	2.884	7.213
230	6.56	2.54	18.67	0.0034	0.433	0.281	4.256	7.142
231	6.56	2.540	25.32	0.0034	0.502	0.240	5.777	8.410
232	6.54	2.540	39.76	0.0034	0.666	0.203	9.117	9.911
233	6.56	3.810	10.	0.0034	0.269	0.210	1.195×10^6	9.779
234	6.56	3.810	13.60	0.0034	0.318	0.189	1.568	10.789
273	6.56	3.810	23.51	0.0034	0.494	0.171	2.718	11.725
274	6.53	5.08	9.110	0.0037	0.291	0.195	3.358	10.377
275	6.52	3.810	35.25	0.0034	0.794	0.184	4.122	11.068
235	5.29	5.081	14.56	0.0034	0.416	0.173	5.296	11.319
001	6.48	5.031	17.54	0.0034	0.523	0.181	6.590	11.120
236	6.69	3.810	57.24	0.0034	1.125	0.159	6.698	12.482
002	6.47	5.081	22.36	0.0034	0.636	0.169	8.400	11.830
237	6.57	5.081	24.76	0.0034	0.589	0.145	9.012	13.768
003	6.46	5.081	27.55	0.0034	0.678	0.149	1.047×10^7	13.420
238	6.56	5.081	38.02	0.0034	0.817	0.130	1.388	14.694
239	6.57	5.081	56.36	0.0034	1.096	0.118	2.047	17.109
240	6.55	5.081	76.00	0.0034	1.319	0.105	2.785	19.051
241	6.53	5.081	92.80	0.0034	1.505	0.098	3.421	20.329
242	6.50	5.081	131.63	0.0034	1.916	0.088	4.900	22.630
243	6.61	7.620	35.73	0.0034	0.648	0.073	6.483	27.263
244	6.63	7.620	49.27	0.0034	0.834	0.068	8.888	29.230
119	6.46	10.16	23.42	0.0045	0.603	0.078	1.410×10^8	25.628
245	6.24	7.620	69.51	0.0034	1.108	0.065	1.435	31.086
120	6.46	10.16	40.36	0.0045	0.877	0.066	2.438	31.016
246	6.63	10.16	48.73	0.0034	1.052	0.065	2.781	30.288
122	6.44	10.16	59.16	0.0040	1.224	0.063	3.60	31.890
247	6.61	10.16	73.54	0.0034	1.311	0.054	4.215	36.762
123	6.44	10.16	93.82	0.0040	1.496	0.048	5.718	41.270
124	6.414	10.16	127.05	0.0040	1.941	0.046	7.804	43.247
125	6.41	10.16	146.47	0.0040	2.107	0.044	9.013	45.783
126	6.40	10.16	186.55	0.0040	2.447	0.039	1.150×10^9	50.186
127	6.36	10.16	235.64	0.0040	2.957	0.038	1.475	50.904

Run	Pr	L (cm)	P (W)	W	ΔT (°C)	$\dfrac{\Delta T}{(\overline{HL^2/2k})}$	Ra	Nu_1
128	6.32	10.16	298.80	0.0040	3.395	0.035	1.893×10^9	57.750
129	6.33	10.16	310.00	0.0040	3.544	0.035	1.958	57.375
253	6.56	17.78	40.30	0.0040	0.783	0.034	2.209	58.949
130	6.32	10.16	385.0	0.0040	4.197	0.033	2.440	60.139
131	6.30	10.16	470.0	0.0040	4.826	0.031	2.998	63.860
132	6.21	10.16	544.0	0.0040	5.751	0.032	3.578	61.910
254	6.56	17.78	72.00	0.0040	1.321	0.032	3.948	62.857
133	5.82	10.16	680.0	0.0040	6.459	0.029	5.114	68.390
137	6.34	12.70	325.0	0.0099	4.158	0.031	5.010	64.010
248	6.35	12.70	360.0	0.0051	4.110	0.028	5.515	71.754
138	6.28	12.70	445.0	0.0099	5.012	0.028	7.004	72.636
249	6.30	12.70	500.0	0.0051	5.549	0.027	7.799	73.780
255	6.51	17.80	141.0	0.0040	2.389	0.029	7.874	68.049
139	6.22	12.70	600.0	0.0099	6.367	0.026	9.647	77.031
262	6.47	25.40	45.00	0.0028	0.881	0.024	1.057×10^{10}	83.897
250	5.69	12.70	640.0	0.0051	7.213	0.028	1.224	71.948
256	6.45	17.78	257.0	0.0040	3.813	0.026	1.460	77.336
251	5.67	12.70	772.0	0.0051	7.981	0.026	1.498	78.370
140	5.13	12.70	772.5	0.0099	7.323	0.024	1.789	84.370
252	5.61	12.70	940.0	0.0051	9.231	0.024	1.850	82.442
257	6.43	17.78	356.0	0.0040	4.479	0.022	2.038	91.295
263	6.47	25.40	93.00	0.0028	1.541	0.020	2.209	99.224
258	6.39	17.78	458.0	0.0040	5.390	0.020	2.661	97.486
259	6.34	17.78	548.0	0.0040	6.281	0.019	3.236	100.01
260	6.16	17.78	620.0	0.0040	7.010	0.019	3.890	101.19
264	6.40	25.40	175.0	0.0028	2.611	0.018	4.214	109.91
261	5.82	17.78	752.0	0.0040	8.480	0.019	5.303	100.89
265	6.36	25.40	278.0	0.0028	3.751	0.016	6.788	121.69
266	6.29	25.40	405.0	0.0028	4.928	0.015	1.012×10^{11}	134.53
208	6.17	25.40	440.0	0.0028	5.432	0.015	1.146	132.97
267	6.25	25.40	524.0	0.0028	5.953	0.014	1.331	143.90
268	6.20	25.40	600.0	0.0028	6.847	0.014	1.546	143.27
269	5.93	25.40	690.0	0.0028	7.811	0.014	1.951	143.74
209	5.07	25.40	702.0	0.0028	6.134	0.011	2.652	184.54
270	5.50	25.40	912.0	0.0028	9.062	0.012	2.981	162.64
215	4.73	25.40	895.0	0.0024	8.306	0.012	3.796	171.40
271	4.99	25.40	1092.0	0.0028	10.47	0.011	4.239	167.01
272	4.96	25.40	1100.0	0.0028	11.54	0.013	4.313	152.57
210	4.31	25.40	1020.0	0.0028	8.074	0.010	4.987	200.45
216	4.43	25.40	1050.0	0.0024	9.994	0.011	4.936	170.12
217	4.28	25.40	1180.0	0.0024	10.78	0.011	5.845	172.83
218	4.23	25.40	1220.0	0.0024	10.84	0.011	6.146	177.53
219	4.08	25.40	1334.0	0.0024	11.11	0.010	7.049	189.33
220	3.92	25.40	1434.0	0.0024	11.87	0.010	8.016	189.72
221	3.77	25.40	1548.0	0.0024	12.97	0.010	9.121	186.76
222	3.74	25.40	1616.0	0.0024	13.17	0.010	9.639	191.81

Run	Pr	L (cm)	P (W)	w	ΔT (°C)	$\dfrac{\Delta T}{(HL^2/2k)}$	Ra	Nu_1
223	3.59	25.40	1740.0	0.0024	13.62	0.010	1.092×10^{12}	198.82
224	3.50	25.40	1810.0	0.0024	12.11	0.009	1.232	230.25
225	3.23	25.40	2000.0	0.0024	14.30	0.009	1.418	214.63
226	3.09	25.40	2120.0	0.0024	15.73	0.009	1.573	205.93
227	2.98	25.40	2272.0	0.0024	16.81	0.009	1.754	205.91
228	2.88	25.40	2360.0	0.0024	17.55	0.009	1.884	204.29
229	2.75	25.40	2468.0	0.0024	17.68	0.009	2.165	222.50

APPENDIX C

ADDITIONAL HEAT TRANSFER CORRELATIONS

The heat transfer data of the present study may also be represented by the following correlations:

$$Nu_1 = 0.221 \ Ra^{1/4} , \qquad (C-1)$$

for the same range of Ra, Pr, and layer aspect ratio, L/X, in Eq. (3).

In the runs at the highest Rayleigh numbers, the mean temperature of the fluid layer often reached values of the order of 50-70°C. Prandtl number variations were then somewhat significant. Thus a correlation of the form

$$Nu_1 = C \ Ra^m Pr^n \qquad (C-2)$$

was also computed. The regression analysis gave for the range of data of Eq. (3) the following:

$$Nu_1 = 0.233 \ Ra^{0.233} Pr^{0.239} . \qquad (C-3)$$

Equation (C-3) represents another correlation of the experimental data which may prove useful at high Rayleigh numbers with Prandtl number variations in the range of the present study. However, Eq. (3) should be used if heat transfer is needed over a wide range of Rayleigh numbers. Most of the data of the present study were obtained with $Pr \approx 6.5$, and Eq. (3) is heavily weighted to this Prandtl number value as a result. The correlations given by Eqs. (3) and (C-3) were obtained with a weight of unity assigned to each data point.

Finally a correlation of the form

$$(Nu_1 - 2) = C(Ra - Ra_c)^m \qquad (C-4)$$

was made for the data of the present study and the data of the Kulacki, et al.[3] By using $Ra_c = 1314$, which is obtained from Eq. (6), this correlation is

$$(Nu_1 - 2) = 0.0787(Ra - 1314)^{0.298} . \qquad (C-5)$$

APPENDIX D

ANALYSIS OF EXPERIMENTAL ERRORS

Because of uncertainties in the parameters used to calculate the Rayleigh number and Nusselt number these dimensionless quantities are subject to a certain amount of error. Both accidental and systematic errors are present.

The accidental error was eliminated in the experiments by taking those measurements which were repeatable several times and taking arithmetic mean values for those readings. Assuming that this method is sufficient to eliminate the accidental error it was assumed that all error resulted from systematic error.

The systematic errors include uncertainties in the thermophysical properties of the electrolyte solution, measurement of power input to the layer, convection cell geometrical dimensions, temperature measurements and the power lost through the bottom plate and sidewalls. Each form of error will be considered in turn. It will be assumed that no error results from concentration gradients of the salt. It is also assumed that the convection cell is perfectly aligned with the horizon.

Applying the law of summation of fractional errors the fractional error in the Rayleigh number is

$$f_{Ra} = f_{properties} + f_{geometric} + f_{power} \, ,$$

and the fractional error in the Nusselt number is

$$f_{Nu} = f_{properties} + f_{geometric} + f_{power} + f_{temperature} \, .$$

The estimated uncertainties in the thermophysical property values are given in Appendix A.

The Mylar covering of the aluminum top plate had an uncertainty of 0.00127 cm which, when added to the 0.00127 cm uncertainty of the Plexiglas plate spacers, resulted in an uncertainty of 0.00254 cm in the fluid layer depth, L. The horizontal dimension of the convection cell is known to within 0.0127 cm. An error of 0.5% was used for all geometrical measurements.

The combined uncertainties in the thermophysical properties and geometrical factors produced an uncertainty of 4 to 6% in the experimental Rayleigh number and 1 to 3% in the experimental Nusselt number.

The accuracy of the wattmeter transducer was rated at 0.25% of reading. Allowing for error of reading the millivolt output of the transducer with the multimeter, the estimated uncertainty in power

consumption was 0.5% for the low Rayleigh number data. For the high Rayleigh number data, the uncertainty in power consumption was estimated to be 1%.

The calculated value of the energy transported through the bottom plate and sidewalls was less than 1% of the measured power input for each run. It is not possible to systematically determine the amount of error in this calculated energy loss because nominal property values supplied by the manufacturer were used in the calculation. Thus, the actual value of energy transported through the top plate was taken to be within 1% of the calculated value.

The uncertainties in the thermocouple output, potentiometer reading, and conversion from emf to degrees Celsius resulted in the error of the measured temperature to be 1%. This gives the most probably error in the temperature difference of 1.5%.

Summing all fractional errors, the error in the Rayleigh number is 5 to 7% and the error in the Nusselt number is 3.5 to 5.5%.

REFERENCES

1. Peckover, R. S., "Experiments on Convection with Internal Heat Sources," UKAEA Research Group Memorandum, CLM-RR/S-2/2, Culham Laboratory, (1973)

2. Peckover, R. S , and Hutchinson, I. M., "Thermal Convection Driven by Internal Heat Sources - An Annotated Bibliography," UKAEA Research Group Report, CLM R-123, Culham Laboratory, (1973).

3. Kulacki, F. A.; Nagle, M. E ; and Cassen, P., "Studies of Heat Source Driven Natural Convection," The Ohio State University Research Foundation, Tech. Rpt. 3746-1, (July, 1974).

4. Kulacki, F. A., and Emara, A. A., "High Rayleigh Number Natural Convection in Enclosed Fluid Layers with Internal Heat Sources," U. S. Nuclear Regulatory Commission, NUREG-75/065, (July, 1975).

5. Kulacki, F. A., and Goldstein, R. J., "Thermal Convection in a Horizontal Fluid Layer with Uniform Volumetric Energy Sources," J. Fluid Mech., 55, 271 (1972).

6. Kulacki, F. A., and Goldstein, R. J., "Hydrodynamic Instability in Fluid Layers with Uniform Volumetric Energy Sources," Appl. Sci. Res., 31, 81 (1975).

7. Baker, L.; Faw, R. E.; and Kulacki, F. A., "Post Accident Heat Removal L: Heat Transfer within an Internally Heated Liquid Layer," submitted for publication to J. Nuc. Sci. and Tech., (in process).

8. Tritton, D. J., and Zarraga, M. N., "Convection in horizontal layers with heat generation. Experiments," J. Fluid Mech., 30, 21 (1967).

9. Schwab, H. J. A., and Schwiderski, E. W., "Convection with electrolitically heated fluid layers, J. Fluid Mech., 48, 703 (1971).

10. Roberts, P. H., "Convection in horizontal layers with internal heat generation. Theory," J. Fluid Mech., 30, 33 (1967).

11. Thirlby, R., "Convection in an internally heated fluid layer," J. Fluid Mech., 44, 673 (1970).

12. Chorin, A., 1967, J. Comp. Phys., 2, 12.